Investigating the characteristics of coronal loop heating by 1-D hydrodynamic simulations

R. Susino[1,2], D. Spadaro[2], A. C. Lanzafame[1,2], A. F. Lanza[2]

[1]Università di Catania, Dipartimento di Fisica e Astronomia

[2]INAF-Osservatorio Astrofisico di Catania

INTRODUCTION

Solving the problem of the heating of the solar corona is presently one of the major issues in solar physics. In particular, the question whether the plasma heating inside coronal loops is the effect of steady or impulsive processes, uniform or localized within the structure, is still open.
While the first models of loop heating (e.g., Rosner et al. 1978; Serio et al. 1981), considering magnetic flux tubes in hydrostatic equilibrium under the effects of steady heating, allow to reproduce quite satisfactorily a large number of characteristics in the X-ray and EUV coronal emission of the Sun, recent TRACE and SOHO observations have provided evidence that a large majority of coronal loops, although appearing in quasi-static conditions, cannot be described by equilibrium models (Porter & Klimchuk 1995, Aschwanden et al. 1999, 2001; Winebarger et al. 2003; Patsourakos et al. 2004).
This issue can be avoided if coronal loops are assumed to consist of unresolved magnetic strands, each of them heated impulsively and non-uniformly, at different times from its neighbours (Cargill 1994; Klimchuk & Cargill 2001; Spadaro et al. 2003; Cargill & Klimchuk 2004; Patsourakos & Klimchuk 2005; Klimchuk 2006; Klimchuk et al. 2008).
In this Poster we present results from a set of hydrodynamic simulations of coronal magnetic loop strands undergoing different kinds of heating regimes (Susino et al. 2009). Aim of this work is to put some constraints on the physical processes responsible for the heating of the coronal structures, by deriving, from the considered hydrodynamic models, diagnostic quantities related to the heating properties, which could successively be compared with detailed observations.

METHODS

The standard set of hydrodynamic equations for the conservation of mass, momentum, and energy of the plasma in a one-dimensional magnetically confined loop are solved with ARGOS, a 1-D hydrodynamic code with fully adaptive-grid package, PARAMESH (Antiochos et al. 1999, MacNeice et al. 2000). A fully adaptive-grid is essential to resolve evolving regions of steep gradients, in this case the thin chromospheric-coronal transition region sections of the loop.
The loop is initially settled into a quasi-static equilibrium state with maximum temperature $T_{max} = 7.5 \times 10^5$ K; subsequently, an additional heating is switched on in the coronal segment of the loop. The additional heating can have different temporal and spatial distributions; we contrasted steady vs. impulsive and uniform vs. asymmetric, localized heating.

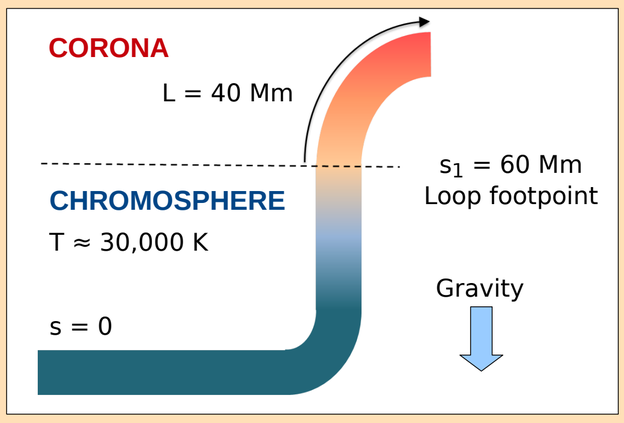

Fig. 1: *Geometry of the loop. It consists in an arched magnetic flux tube of coronal semi-length L = 40 Mm and apex height above the chromosphere h = 15 Mm. At each footpoint (s_1), there's a 60 Mm long chromospheric segment, acting as a mass reservoir and maintained at a constant temperature of 30,000 K.*

In the localized-heating cases, the heating rate function H(s,t) decreases exponentially from the footpoint to the loop top, with a scale-length λ = 10 Mm. In the impulsive-heating cases, the Maxwellian-shaped energy pulses (nanoflares) have all the same duration and energy amplitude (see Fig. 2). The time interval between consecutive pulses, the cadence t_C, is kept constant throughout each run. The heating-rate applied to the chromosphere is maintained uniform and steady in all cases. We run simulations varying the cadence t_C (with respect to the radiative cooling-time of the loop, $\tau_{cool} \approx 1000$ s) and the amount of energy E_P injected into the loop in a time interval equal to t_C.

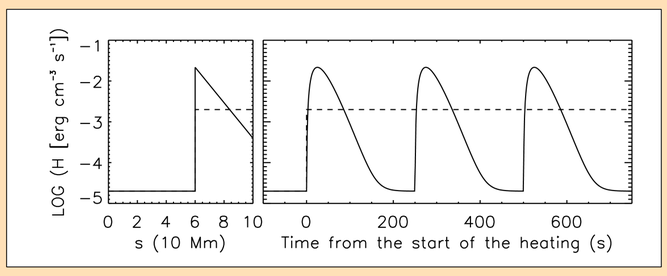

Fig. 2. Left: *Heating-rate function vs. the curvilinear coordinate s along half of the loop, for localized (solid line) and uniform (dashed line) heating.* **Right:** *Heating-rate function vs. time, for impulsive heating with t_C = 250 s (solid line) and steady heating (dashed line).*

PLASMA DYNAMICS

In the uniform-heating regimes, both steady and impulsive, the model settles into a new quasi-static equilibrium state (see Fig. 3a, left panels). The time-averaged apex temperature and density for this new state are consistent with the hydrostatic scaling laws of Rosner et al. (1978). When $t_C > \tau_{cool}$ (Fig. 3a, left panels, yellow lines), the temperature and velocity in the upper part of the loop exhibit more pronounced oscillations than the case $t_C << \tau_{cool}$, since there is enough time between pulses for the plasma to cool down.
Conversely, asymmetric, localized heating causes a more dynamic evolution (see Fig. 3a, right panels). When the heating is steady, or impulsive with $t_C << \tau_{cool}$ (Fig. 3a, right panels, blue and red lines), the temperature and density curves present long-term fluctuations due to cycles of plasma condensation formation. The condensation is the effect of a thermal instability that develops near the loop top, where the energy supply is not sufficient to balance the radiative losses enhanced by the strong chromospheric evaporation. This leads to a progressive cooling of the material located close to the loop apex, and to the formation of a condensation, that successively moves towards the less heated footpoint of the loop and drains onto the chromosphere (this is well visible from the density profiles in Fig. 3a, right panels, blue and red lines). Plasma condensation does not form when the cadence is comparable to or exceeds τ_{cool} (Fig. 3a, right panels, yellow lines), or for high-energy regimes ($E_P = 2 \times 10^{24}$ erg; see Fig. 3a, green lines); in these cases the behaviour is closer to that of the uniform-heating cases.
The plot of <n> vs. <T> (Fig. 3b) shows that in the uniform-heating cases the plasma filling the loop is prevalently under-dense with respect to the hydrostatic equilibrium during the initial phase of the heating, then it approaches a new quasi-static equilibrium when $t_C << \tau_{cool}$ (Fig. 3b, top panel, blue and red lines) or oscillates in a wide region around the equilibrium when the cadence exceeds the radiative cooling time (Fig. 3b, yellow line).
In the localized-heating cases, after an initial under-dense phase, the representative point of the loop stands most of the time in the over-dense region during the condensation cycles when they occur (Fig. 3b, bottom panel, blue and red lines), while it reaches quasi-static conditions or oscillates around the equilibrium when condensation does not form (Fig. 3b, bottom panel, green and yellow lines, respectively).

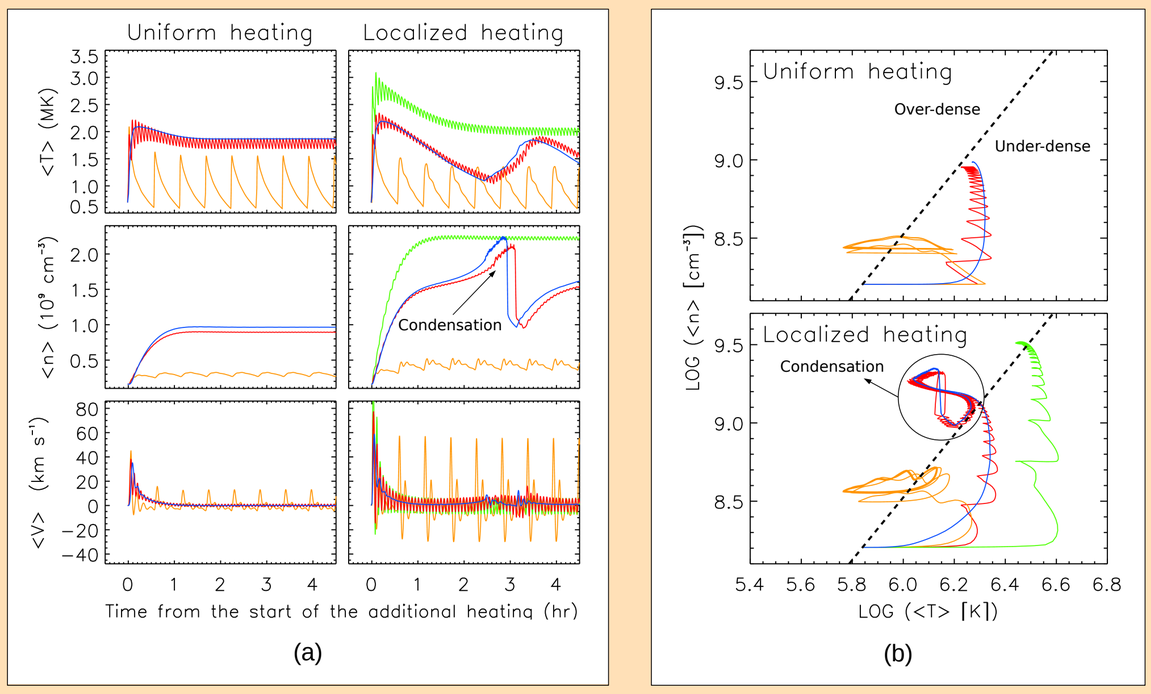

Fig. 3. (a) *Initial part of the temporal evolution of the loop temperature (top panel), density (middle panel), and velocity (bottom panel), averaged over the upper ¾ of the loop, for uniform (left panels) and localized (right panels) heating, in representative cases: steady heating with $E_P = 10^{24}$ erg (blue line), impulsive heating with $E_P = 10^{24}$ erg (t_C = 250 s, red line; t_C = 2000 s, yellow line), and impulsive heating with $E_P = 2 \times 10^{24}$ erg and t_C = 250 s (green line).* **(b)** *Average loop density as a function of the average temperature for the same runs. The black dashed line connects the hydrostatic equilibrium loci as given by the theoretical scaling laws (see Rosner et al. 1978), gauged according to the initial state of our models.*

PLASMA DIAGNOSTICS

From the set of hydrodynamic variables n(s), T(s), and v(s) calculated by our code, we reconstructed, for each run, the emission line profiles of the O V (629.7 Å) and Mg X (609.8 Å) lines (assuming ionization equilibrium). We simulated a multi-strand loop observation by averaging instantaneous line profiles calculated at N = 300 different times, randomly selected throughout each simulation. Although a run represents the evolution of a single magnetic strand, we assume that the states of the model at N randomly selected times can be used to describe the behaviour of N independent strands observed at the same time. From the average profile obtained in this way, we successively derived the Doppler-shifts for both the spectral lines. We used the same approach to compute the differential emission measure, DEM(T) (see, e.g., Craig & Brown 1976), which effectively describes the plasma distribution in temperature. The results are shown in Fig.s 4 and 5, respectively.

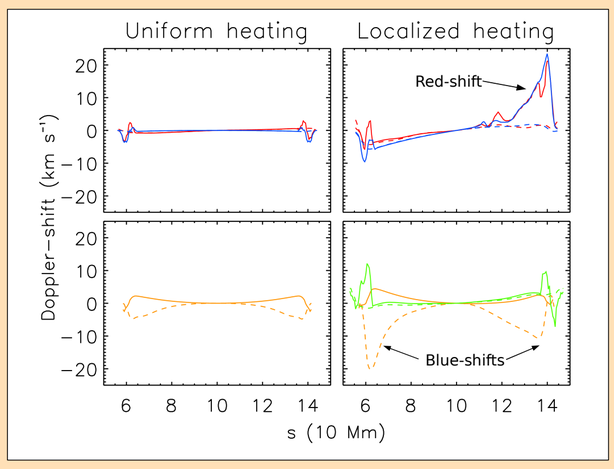

Fig. 4 *O V (solid lines) and Mg X (dashed lines) average Doppler-shifts, plotted as a function of the loop coordinate s for the same runs as in Fig. 3 (marked with the same colours). Positive velocities correspond to red-shifts, i.e., to down-flows.*

The Mg X line exhibits pronounced blue-shifts (up to 20 km s^{-1}), located near the loop footpoints, only when the cadence t_C exceeds the radiative cooling time (Fig. 4, right panels, yellow dashed line), otherwise it seems not to be strongly influenced by the characteristics of the heating.
The DEM curves obtained from our models (Fig. 5) appear not to be sensitive to the condensation process, since they show very similar trends, irrespective of the spatial properties of the heating. The position of the coronal DEM peak, as well as its amplitude, depend on the mean energy injected into the loop (<E> ≈ E_P / t_C): the larger <E>, the higher is the peak and the more it is shifted towards higher temperatures. The shape of the coronal portion of the DEM (for LOG T > 5.5) seems to be related to the pulse cadence t_C: when $t_C > \tau_{cool}$ the rather pronounced coronal peak visible in the high-cadence DEM curves tends to disappear (compare, e.g., the green, blue/red, and yellow curves in Fig. 5, bottom panel).

The Doppler-shift curves for both the Mg X and O V lines do not show, as expected, appreciable variations in the uniform-heating cases (Fig. 4, left panels), due to the rather low velocities that characterize these runs.
In the localized-heating cases, conversely, the O V line appears to be strongly red-shifted (with velocities up to 25 km s^{-1}) in the runs that develop a condensation (Fig. 4, right panels, blue and red solid lines), the maximum being located within the less heated leg of the loop, where the condensation forms and drains. No significant variations in the O V Doppler velocity are found for the condensation-free runs, apart from moderate shifts (less than 10 km s^{-1}) near both the loop footpoints.

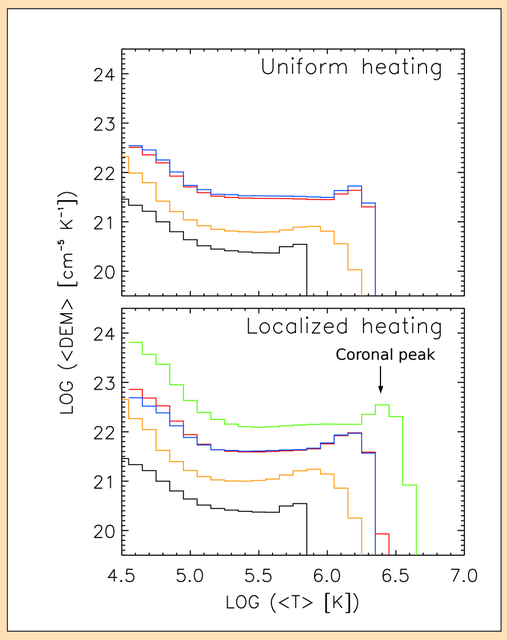

Fig. 5 *Time-averaged differential emission measure (DEM) computed for the same runs of Fig.s 3 and 4. The black curve is the DEM obtained for the initial state.*

CONCLUSIONS

Our modelling of multi-stranded coronal loops shows that the variation of the spatial and temporal heating characteristics can influence the dynamic behaviour of the plasma and have observable consequences. Asymmetric, localized heating causes, in general, a more dynamic evolution of the loop than uniform heating, with, in particular, the onset of plasma condensation cycles when the heating is steady or impulsive with $t_C << \tau_{cool}$. The O V line, representative of transition-region lines, appears to be sensitive to the condensation process, since it marks the down-flows of the cool plasma filling the condensation, during the draining phase. Conversely, the Mg X line, representative of coronal lines, exhibits significant blue-shifts located near the loop footpoints only when the loop is impulsively heated with $t_C > \tau_{cool}$, as a consequence of the strong chromospheric evaporation taking place therein. However, since ionization non-equilibrium effects can affect the observed line emission, a further analysis is needed including also ionization non-equilibrium in the line profile reconstruction. The DEM response to the different heating regimes seems to be rather low; however, an appreciable sensitivity to the pulse cadence is found in the impulsive case when $t_C > \tau_{cool}$, for which the differences induced in the DEM shape can be larger than the uncertainties. The future comparison of the results obtained in this study with observations could help in discriminating, at least in some cases, what kind of heating regime is at work.

REFERENCES

Antiochos, S.K., MacNeice, P.J., Spicer, D.S., & Klimchuk, J.A. 1999, ApJ, 512, 985
Aschwanden, M.J., Newmark, J S., Delaboudinière, J.-P., Neupart, W.M., Klimchuk, J.A., Gary, G.A. et al. 1999, ApJ, 515, 842
Aschwanden, M., Schrijver, C.J., & Alexander, D. 2001, ApJ, 550, 1036
Cargill, P.J. 1994, ApJ, 422, 381
Cargill, P.J. & Klimchuk, J. A. 2004, ApJ, 605, 911
Craig, I. J.D. & Brown, J.C. 1976, A&A, 49, 239
Klimchuk, J.A. 2006, Sol. Phys., 234, 41
Klimchuk, J.A., Patsourakos, S., & Cargill, P.J. 2008, ApJ, 682, 1351
Klimchuk, J.A. & Cargill, P. J. 2001, ApJ, 553, 440
MacNeice, P.J., Olson, K.M., Mobarry, C., de Fainchtein, R., & Packer, C. 2000, Comput. Phys. Commun., 126, 330
Patsourakos, S., Klimchuk, J.A., & MacNeice, P.J. 2004, ApJ, 603, 322
Patsourakos, S. & Klimchuk, J.A. 2005, ApJ, 628, 1023
Porter, L. J. & Klimchuk, J. A. 1995, ApJ, 454, 499
Rosner, R., Tucker, W. H., & Vaiana, G.S. 1978, ApJ, 220, 643
Serio, S., Peres, G., Vaiana, G.S., Golub, L., & Rosner, R. 1981, ApJ, 243, 288
Spadaro, D., Lanza, A. F., Lanzafame, A. C., Karpen, J. T., Antiochos, S. K., Klimchuk, J. A., & MacNeice, P. J. 2003, ApJ, 582, 486
Susino, R., Lanzafame, A.C., Lanza, A.F. & Spadaro, D. 2009, ApJ *submitted*
Winebarger, A. R., Warren, H. P., & Mariska, J. T. 2003, ApJ, 587, 439